Supplementary Information (SI) for ChemComm.

Efficient Spin-Doublet Near-Infrared Emission Beyond 800 nm via Intramolecular Charge Transfer in Quasi-Planar Donor-Acceptor Structure

Lingfeng Xiang,[a†] Shilong Yu[a†], Xiaotong Ji[a], Yuqi Chen[a], Yusheng Yan[a], Jiashun Feng[a], You-Jun Yu,*[a] Houyu Zhang[a], Ming Zhang[a], Feng Li*[a]

[a] State Key Laboratory of Supramolecular Structure and Materials, College of Chemistry, Jilin University, Changchun 130012, P. R. China.

*E-mail: yjyu@jlu.edu.cn; lifeng01@jlu.edu.cn

Contents

1. General information

All reagents and solvents required for synthesis and characterization are purchased from commercial suppliers and used directly without any treatment.

The nuclear magnetic resonance spectra were recorded on the Bruker AVANCEIII 400 spectrometer at 400 MHz at 298 K with tetramethyl silane (TMS) (δH = 0 ppm) as the internal standard. MALDI-TOF mass spectra were recorded on a Brucker Autoflex speed TOF/TOF mass spectrometer with DCTB as a matrix. Elemental analysis (C, H and N) was performed on a Elementar Vario micro cube elemental analyzer. EPR0020spectra were recorded on a Bruker ELEXSYSII E500 CW-EPR spectrometer at 298K. Thermal gravimetric analysis (TGA) was characterized by a TAINSTRUMENTS Q500 TGA analyzer. at a heating rate of 10 °C/min under nitrogen, the temperature at 5% weight loss was used as the decomposition temperature (T_d). The electrochemical oxidation and reduction potentials were recorded using an electrochemical analyzer (CHI660C, CH Instruments, USA). A conventional three-electrode configuration consisting of a platinum working electrode, a Pt-wire counter electrode, and an Ag/AgCl reference electrode was used. The solvent in the measurement was CH_2Cl_2, and the supporting electrolyte was 0.1 M tetrabutylammonium hexafluorophosphate. Ferrocene was added as a calibrant after each set of measurements, and all potentials reported were quoted regarding the ferrocene-ferrocenium (Fc/Fc^+) couple at a scan rate of 100 mV/s. UV–vis absorption spectra were recorded on the model UV-vis-2550 spectrophotometer. The Fluorescence spectra, fluorescence decay spectra and PLQE were recorded on an Edinburgh fluorescence spectrometer (FLS980), and the lifetime of the excited states was measured by the time correlated single photon counting method under the excitation of a laser (378 nm). Photostability of radicals was tested under a 365 nm UV lamp irradiation.

Quantum simulations were performed on Gaussian16 [1] series of programs at PBE0/def2svp level. Multiwfn [2] and VMD [3] were utilized to analyze the simulation results

2. **Synthesis and characterization**

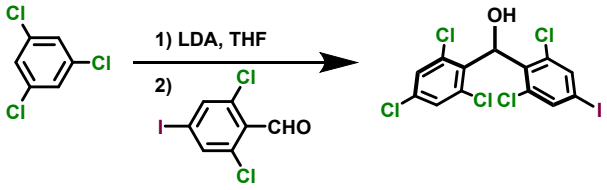

Under argon conditions, 1,3,5-trichlorobenzene (5.00 g, 27.56 mmol) was dissolved in anhydrous tetrahydrofuran (THF, 100 mL) and cooled to -78 °C. Then, LDA (2.00 M, 15.16 mL,30.31 mmol) was slowly added at -78 °C. After stirring for 1 hour at -78 °C, 2,6-dichloro-4-iodobenzaldehyde (9.12 g, 30.31 mmol) was added. The reaction mixture was maintained at -78 °C for an additional 2 h, then allowed to warm to room temperature. The reaction was quenched with a saturated aqueous ammonium chloride solution. The product was extracted with dichloromethane several times, and the combined organic phases were dried over anhydrous magnesium sulfate. The solvent was removed under reduced pressure to afford the crude product, which was subsequently purified by silica gel column chromatography (petroleum ether/dichloromethane = 3:1, v/v). 13.00 g (yield 97.80%) white solid was obtained. The NMR and MS spectra were consistent with those reported in the literature. [4]

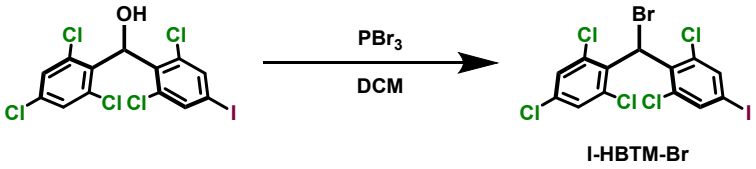

I-HBTM-Br

Under argon conditions, (2,6-Dichloro-4-iodophenyl) (2,4,6-trichlorophenyl) methanol (5 g, 10.37 mmol) was dissolved in a solution of anhydrous dichloromethane (100 mL) and cooled to 0 °C. Then, phosphorus tribromide (2.44 mL, 25.91 mmol) in dry dichloromethane (10 mL) was added dropwise. After that, the reaction mixture was warmed to room temperature and refluxed for 12 h. After the reaction was cooled to room temperature, it was slowly poured into water (200 mL). The mixture was extracted with dichloromethane several times. The combined organic solution was washed with brine and dried over anhydrous sodium sulfate. The solvent was removed under reduced pressure to afford the crude product, which was subsequently purified by silica gel column chromatography (petroleum ether). 5.00 g (yield 88.46%) of white solid (**I-HBTM-Br**) was obtained. **MALDI-TOF (m/z)**: Calcd for $C_{13}H_5BrCl_5I$ $[M]^+$ 543.7032; Found $[M]^+$ 543.8046.

^1H NMR (400 MHz, $CDCl_3$) δ 7.67 (s, 1H), 7.35 (s, 1H), 7.05 (s, 1H). ^{13}C NMR (126 MHz, $CDCl_3$) δ 138.26, 136.97, 136.88, 134.73, 133.17, 131.98, 129.80, 93.04, 41.97.

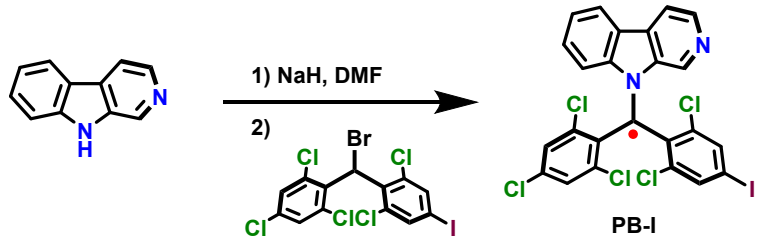

Under argon conditions, PyID (1.39 g, 8.25 mmol), sodium hydride (60% in oil, 0.26 g, 11 mmol) was dispersed in anhydrous N,N-dimethylformamide (50 mL) and stirred at room temperature for 1 h. After **I-HBTM-Br** (3 g, 5.50 mmol) was added, the reaction mixture was heated at 80 °C for 3 h. After cooling to room temperature, the mixture was poured into a saturated sodium chloride solution (100 mL). The crude product was collected by suction filtration, which was subsequently purified by silica gel column chromatography (ethyl acetate: petroleum ether = 1:16, v/v). 0.50 g (yield 14.39%) deep-red solid are obtained. **MALDI-TOF (m/z)**: Calcd for $C_{24}H_{11}Cl_5IN_2$• $[M]^+$ 630.838; Found $[M]^+$ 630.831.

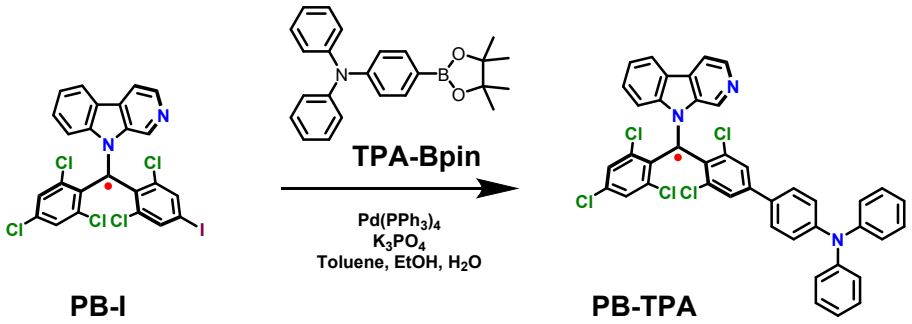

Under argon conditions, N,N-diphenyl-4-(4,4,5,5-tetramethyl-1,3,2-dioxaborolan-2-yl)aniline (TPA-Bpin, 0.52 g, 1.39 mmol), PB-I (0.80 g, 1.27 mmol), potassium phosphate (2.15 g, 10.16 mmol), and tetra-(triphenylphosphine) palladium (0.08 g, 0.06 mmol) were dissolved in a 28 mL mixture solvent (toluene/ethanol/water = 4/1/2, v/v/v). The reaction mixture was heated at 80 °C for 48 h. After the reaction was complete, the reaction mixture was extracted several times with dichloromethane. The combined organic phase was then dried with anhydrous $MgSO_4$. The solvent was removed under reduced pressure to afford the crude product, which was subsequently purified by silica gel column chromatography (petroleum ether/ethyl acetate = 2/1, v/v). 0.80 g (84.32%) dark-purple solid was obtained. **MALDI-TOF (m/z)**: Calcd for $C_{42}H_{25}Cl_5N_3$• $[M]^+$ 748.9330; Found $[M]^+$ 749.0540. **Elem. Anal.** Calcd for $C_{42}H_{25}Cl_5N_3$•: C 67.36, H 3.36, N 5.61; Found: C 68.42, H 3.51, N 5.40.

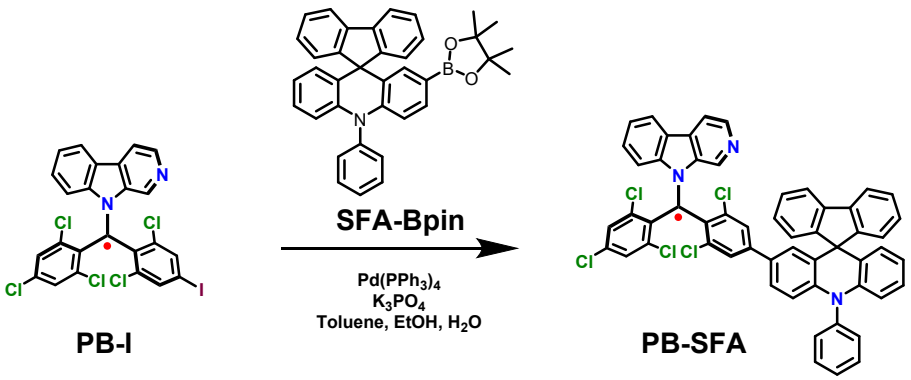

Under argon conditions, 10-phenyl-2-(4,4,5,5-tetramethyl-1,3,2-dioxaborolan-2-yl)-10H-spiro[acridine-9,9'-fluorene](0.74 g 1.39 mmol) (SFA-Bpin), PB-I (0.8 g, 1.27 mmol), potassium phosphate (2.15 g, 10.16 mmol), tetra-(triphenylphosphine) palladium (0.08 g,0.06 mmol), and tetra-(triphenylphosphine) palladium (0.08 g, 0.06 mmol) were dissolved in a 28 mL mixture solvent (toluene/ethanol/water = 4/1/2, v/v/v). The reaction mixture was heated at 80 °C for 48 h. After the reaction was complete, the reaction mixture was extracted several times with dichloromethane. The combined organic phase was then dried with anhydrous $MgSO_4$. The solvent was removed under reduced pressure to afford the crude product, which was subsequently purified by silica gel column chromatography (petroleum ether/ethyl acetate = 2/1, v/v). 0.92 g (79.71%) dark-purple solid are obtained. **MALDI-TOF (m/z)**: Calcd for $C_{55}H_{31}Cl_5N_3$• $[M]^+$ 911.1240; Found $[M]^+$ 911.1007. **Elem. Anal.** Calcd for $C_{55}H_{31}Cl_5N_3$•: C 72.50, H 3.43, N 4.61; Found: C 73.02, H 3.66, N 4.03.

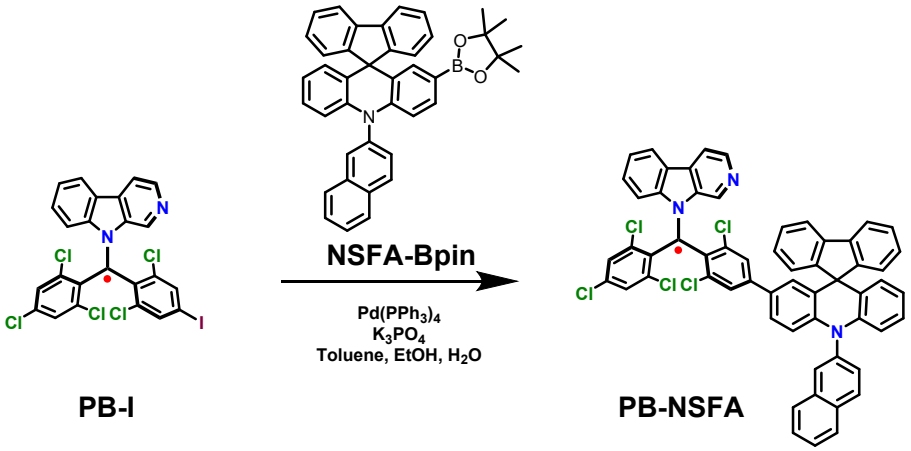

Under argon conditions, 10-(naphthalen-2-yl)-2-(4,4,5,5-tetramethyl-1,3,2-dioxaborolan-2-yl)-10H-spiro[acridine-9,9'-fluorene] (NSFA-Bpin, 0.81 g 1.39 mmol), PB-I (0.80 g, 1.27 mmol), potassium phosphate (2.15 g, 10.16 mmol), tetra-(triphenylphosphine) palladium (0.08 g, 0.06 mmol), and tetra-(triphenylphosphine) palladium (0.08 g, 0.06 mmol) were dissolved in a 28 mL mixture solvent (toluene/ethanol/water = 4/1/2, v/v/v). The reaction mixture was heated at 80 °C for 48 h. After the reaction was complete, the reaction mixture was extracted several times with dichloromethane. The combined organic phase was then dried with anhydrous $MgSO_4$. The solvent was removed under reduced pressure to afford the crude product, which was subsequently purified by silica gel column chromatography (petroleum

ether/ethyl acetate = 2/1, v/v). 0.95 g (78.02%) dark-purple solid are obtained. **MALDI-TOF (m/z)**: Calcd for $C_{59}H_{33}Cl_5N_3$• [M]+ 961.1840; Found [M]+ 961.1162. **Elem. Anal.** Calcd for $C_{59}H_{33}Cl_5N_3$•: C 73.73, H 3.46, N 4.37; Found: C 74.01, H 3.68, N 3.90.

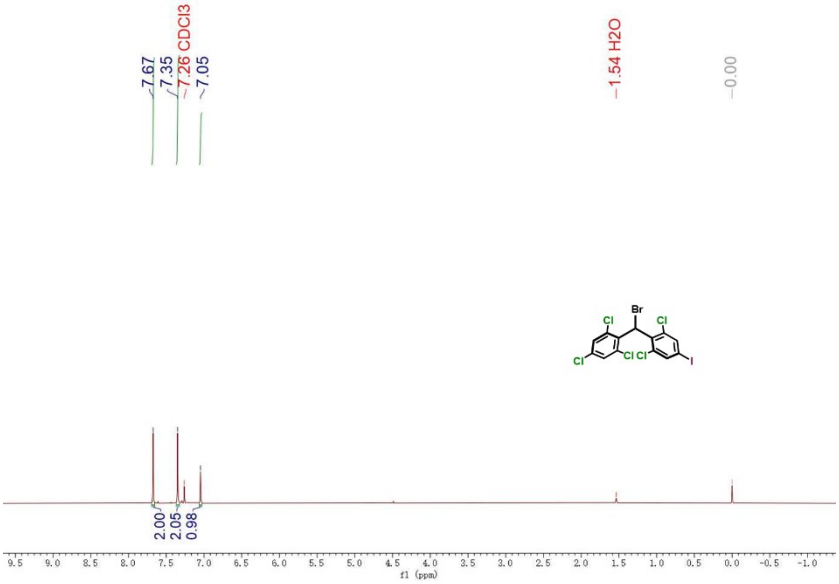

Fig. S1.[1]HNMR spectrum of I-HBTM-Br in $CDCl_3$

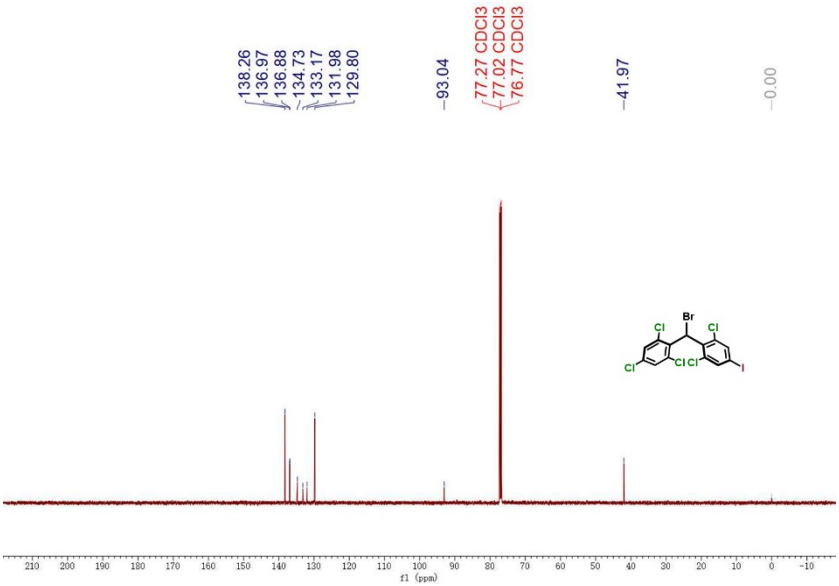

Fig. S2.[13]CNMR spectrum of I-HBTM-Br in $CDCl_3$

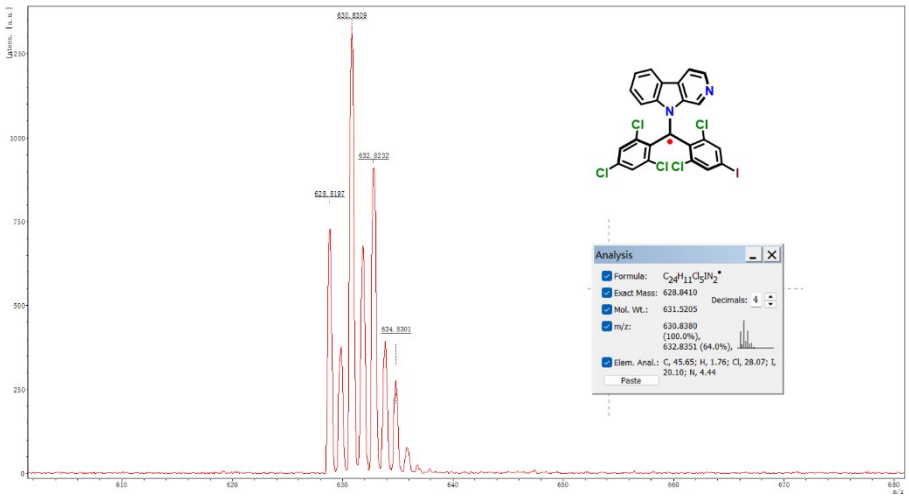

Fig. S3. MALDI-TOF mass spectrum of PB-I.

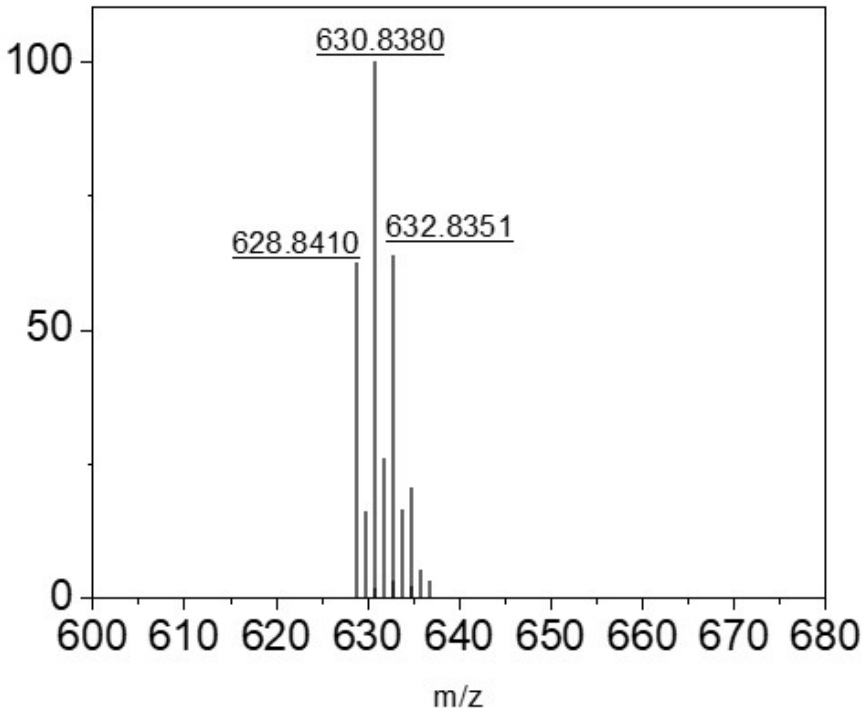

Fig. S4. Simulated MALDI-TOF mass spectrum of PB-I.

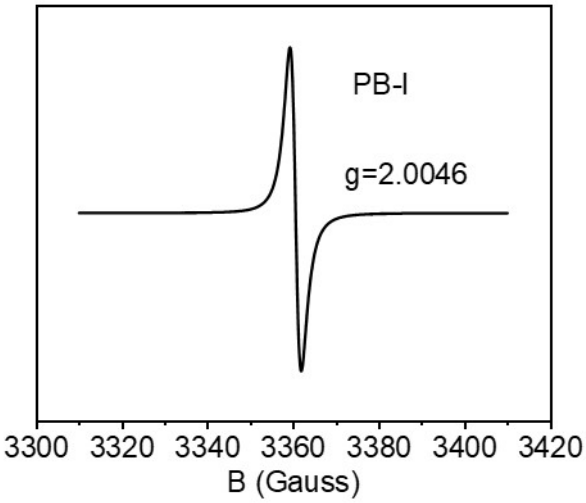

Fig. S5 EPR spectrum of PB-I in chloroform at room temperature.

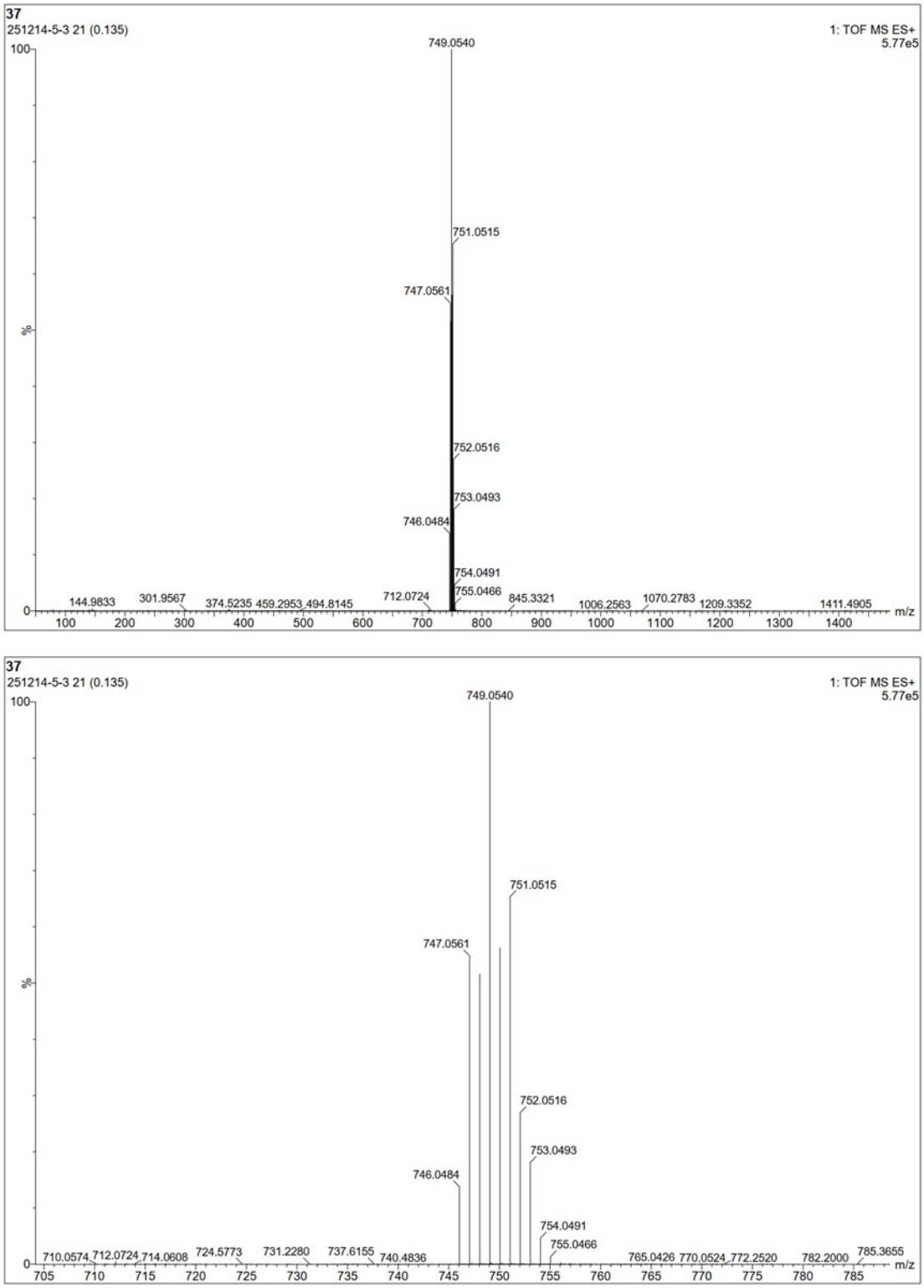

Fig. S6. MALDI-TOF mass spectrum of PB-TPA

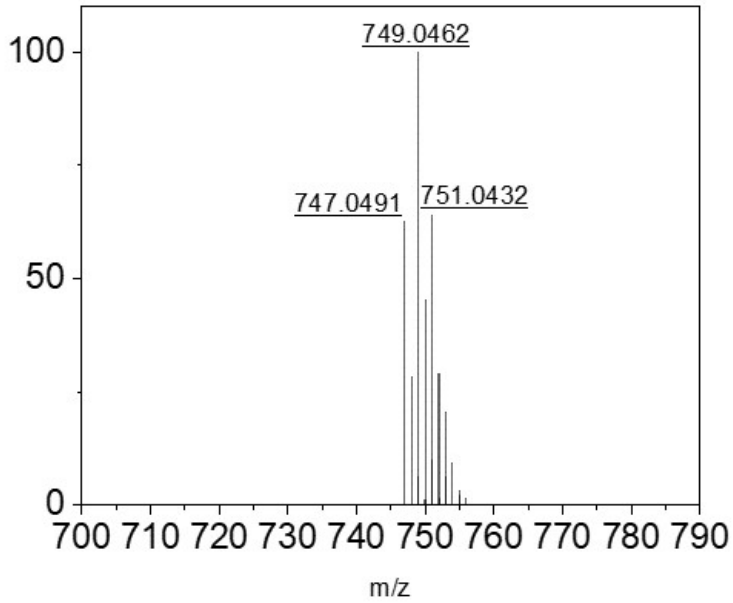

Fig. S7. Simulated MALDI-TOF mass spectrum of PB-TPA.

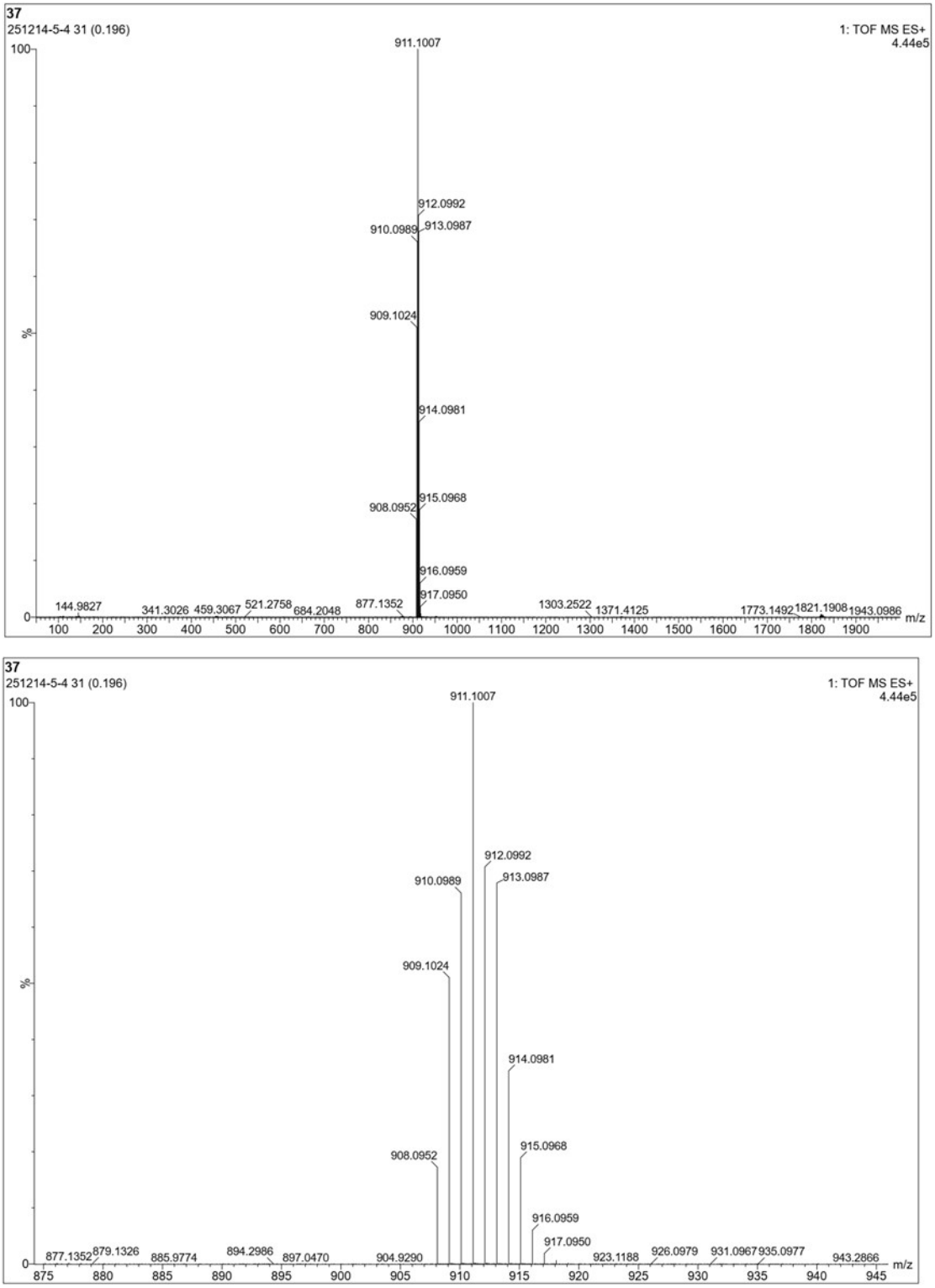

Fig. S8. MALDI-TOF mass spectrum of PB-SFA

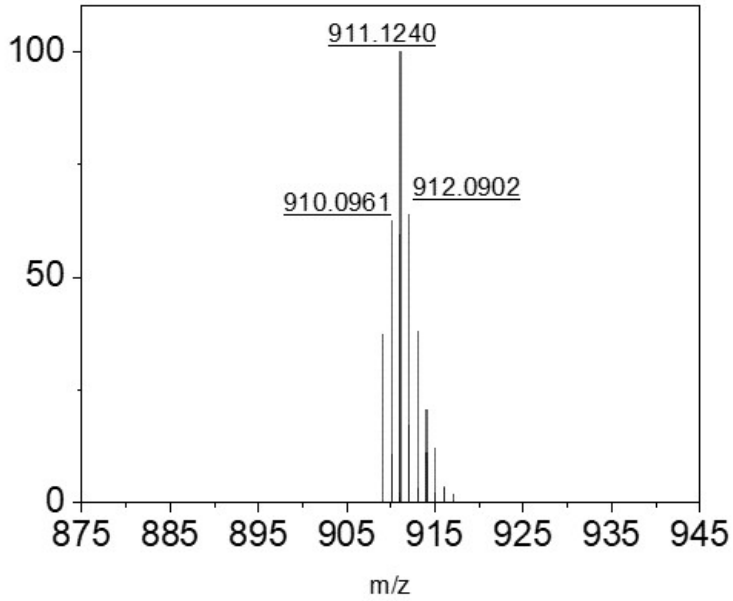

Fig. S9. Simulated MALDI-TOF mass spectrum of PB-SFA

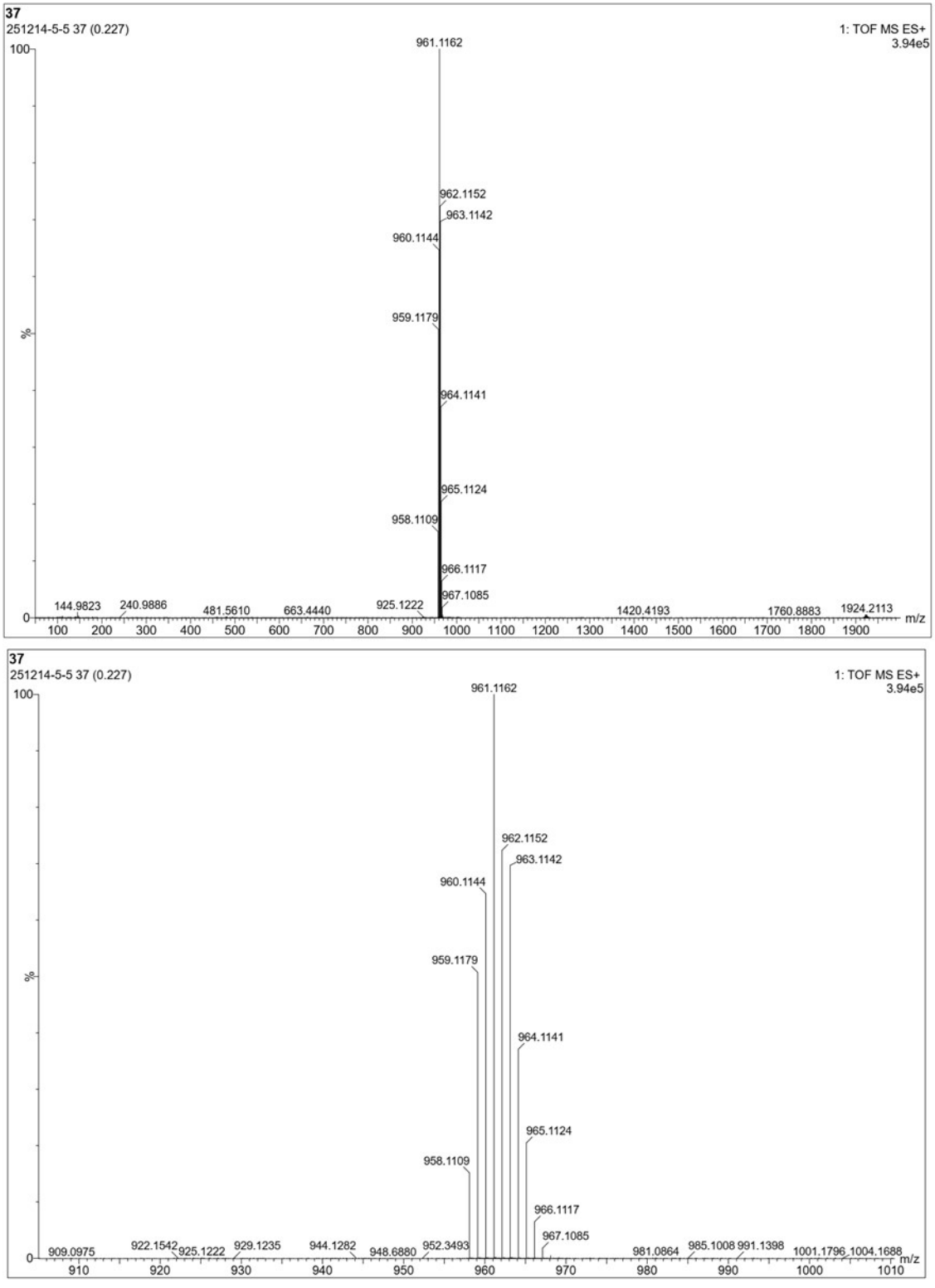

Fig. S10. MALDI-TOF mass spectrum and of PB-NSFA.

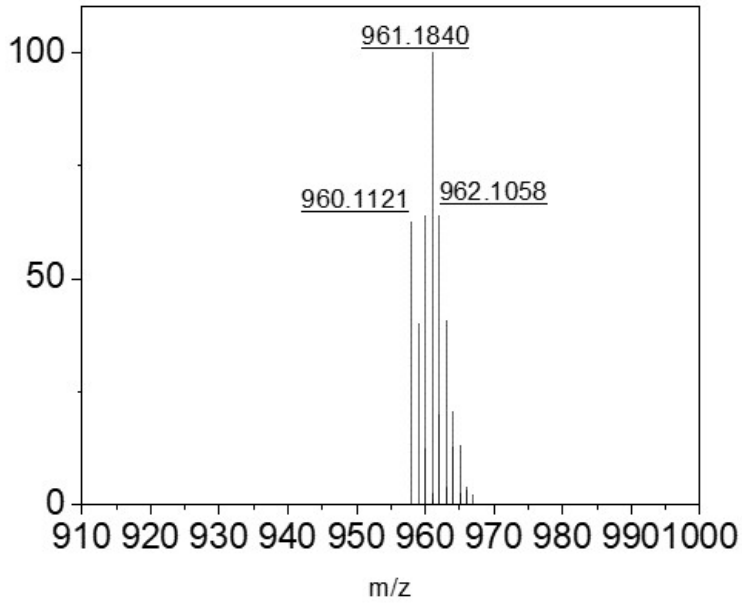

Fig. S11. Simulated MALDI-TOF mass spectrum and of PB-NSFA.

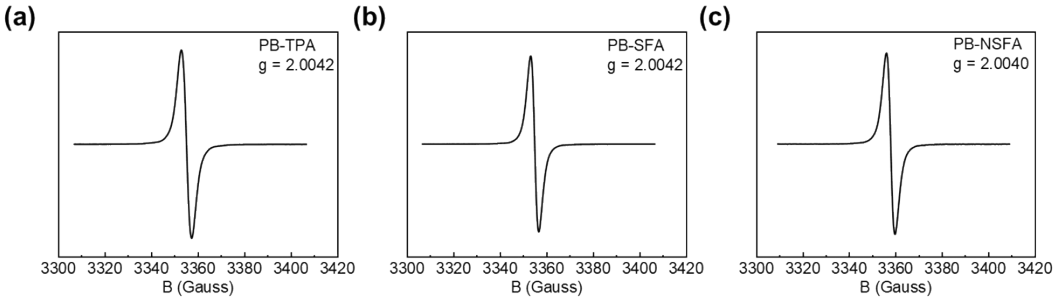

Fig. S12. EPR spectrum of (a) PB-TPA, (b) PB-SFA, and (c) PB-NSFA in chloroform at room temperature.

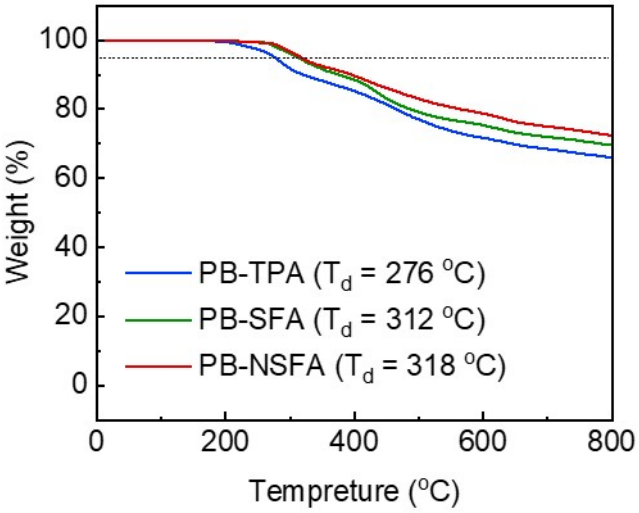

Fig. S13. TGA curves of PB-TPA, PB-SFA, and PB-NSFA.

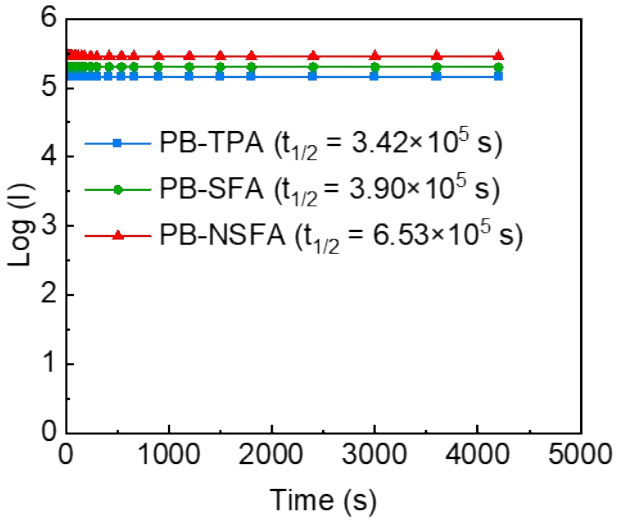

Fig. S14. Comparison of fluorescence decay of PB-TPA, PB-SFA, and PB-NSFA in toluene under irradiation with a 365 nm UV lamp.

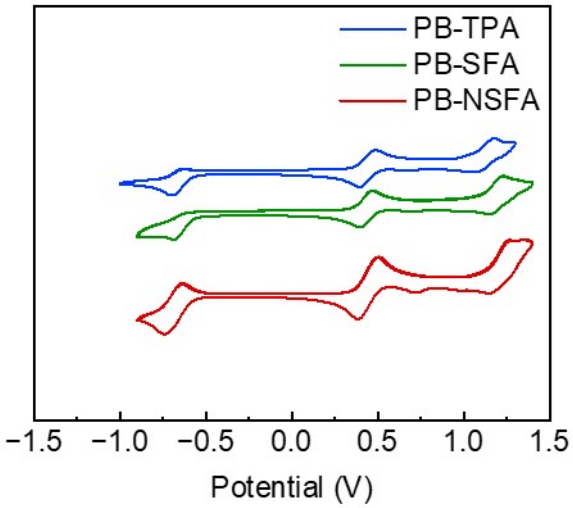

Fig. S15. CV curves of PB-TPA, PB-SFA, and PB-NSFA.

Table S1. The electrochemical parameters and derived orbital energy levels of the three radicals are summarized below

Radical	E_{Ox2}[a] **(V)**	E_{Ox1}[b] **(V)**	E_{Red}[c] **(V)**	$E_{HOMO\beta}$[d] **(eV)**	$E_{SOMO\alpha}$[e] **(eV)**	$E_{SUMO\beta}$[f] **(eV)**	E_g[g] **(eV)**
PB-TPA	1.04	0.37	-0.56	-5.44	-4.77	-3.84	1.60
PB-SFA	1.12	0.39	-0.58	-5.52	-4.79	-3.82	1.70
PB-NSFA	1.13	0.57	-0.67	-5.53	-4.97	-3.73	1.80

[a]The second oxidation peak corresponds to the oxidation of the HOMOβ.

[b]The first oxidation peak is assigned to the oxidation of the SOMOα.

[c]The first reduction peak represents electron injection into the SUMOβ.

[d]HOMOβ, [e]SOMOα, and [f]SUMOβ energy levels were calculated using the formulas $E_{HOMO\beta} = -(E_{Ox2} + 4.4)$ eV, $E_{SOMO\alpha} = -(E_{Ox1} + 4.4)$ eV, and $E_{SUMO\beta} = -(E_{Red} + 4.4)$ eV.

[g]The electrochemical band gap was then derived as $E_g = E_{SUMO\beta} - E_{HOMO\beta}$

3. Photophysical properties

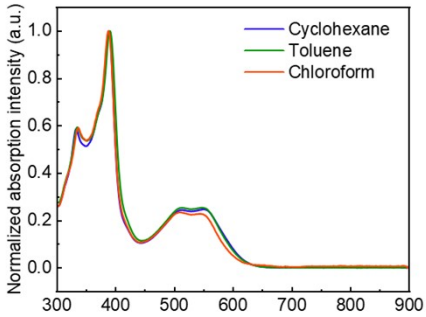

Fig. S16. Absorption spectra of PB-I in various solvents (10^{-5} M) at room temperature.

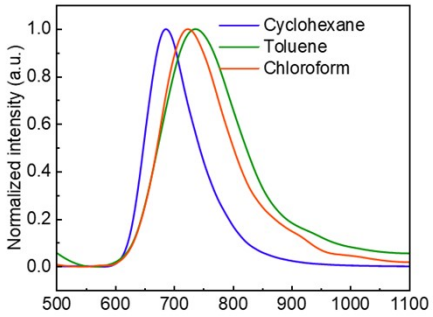

Fig. S17. PL spectra of PB-I in various solvents (10^{-5} M) at room temperature.

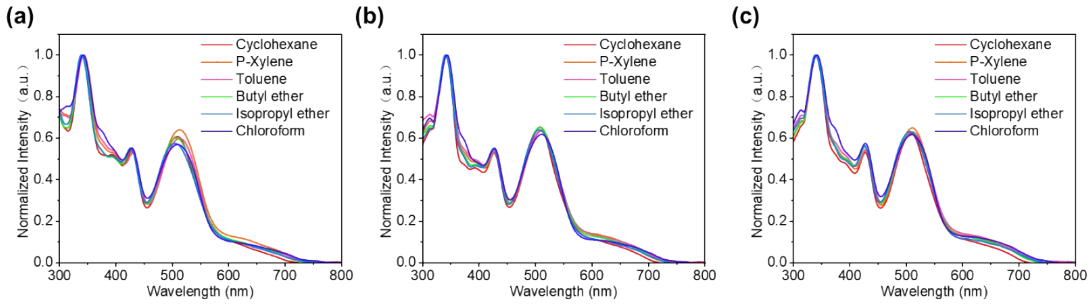

Fig. S18. Absorption spectra of (a) PB-TPA, (b) PB-SFA, and (c) PB-NSFA in various solvents (10^{-4} M) at room temperature.

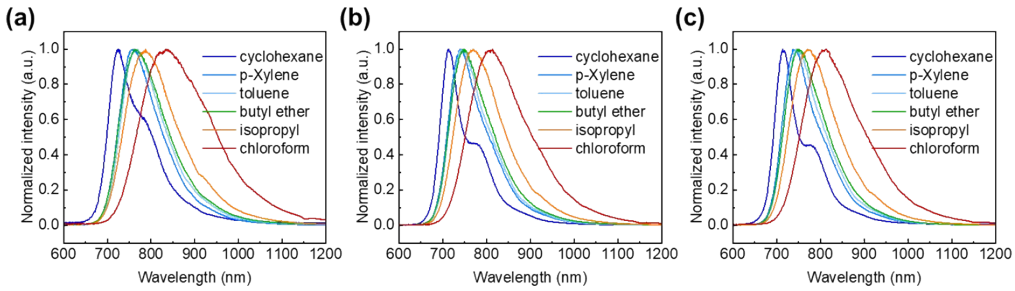

Fig. S19. PL spectra of (a) PB-TPA, (b) PB-SFA, and (c) PB-NSFA in various solvents (10^{-4} M) at room temperature

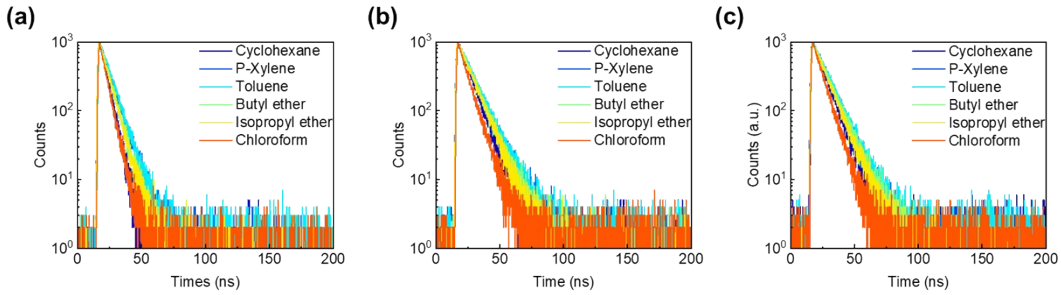

Fig. S20.Transient decay spectra of (a) PB-TPA, (b) PB-SFA, and (c) PB-NSFA in various solvents at room temperature

Table S2. Summarized data on metal-free NIR emissive organic small molecules with photoluminescence (PL) peak in the range above 770 nm.

Molecule	λ_{PL}[a] (nm)	Φ_{sol}[a] (%)	λ_{PL}[b] (nm)	Φ_{film}[b] (%)	Ref.
M1	904 (toluene-d)	15	--	--	[5]
M2	790 (hexane)	16.8	--	--	[6]
M3	895 (hexane)	4.7	--	--	[6]
M4	--	--	830	17	[7]
M5	--	--	820	10.7	[8]
BODIPY dye	**λ_{PL}[a] (nm)**	**Φ_{sol}[a] (%)**			**Ref.**
B1	808 (DCM)	11			[9]
B2	830 (DCM)	1			[10]
B3	816 (toluene)	17			[11]
B4	807 (toluene)	5			[11]
B5	798 (toluene)	2			[12]
B6	810 (toluene)	5			[13]
B7	771 (toluene)	35			[13]
B8	820 (Chloroform)	11			[14]
B9	862 (DCM)	12			[15]
B10	916 (DCM)	2			[15]
B11	814 (Chloroform)	10			[16]
B12	793 (Chloroform)	12			[16]
B13	816 (Chloroform)	4			[16]
B23	807 (Chloroform)	5			[16]
B14	796 (Chloroform)	2			[17]
B15	803 (Chloroform)	5			[17]
B16	774 (Chloroform)	32			[18]
B17	781 (Chloroform)	36			[18]
B18	868 (Chloroform)	4			[18]
B19	861 (Chloroform)	3			[18]
B20	819 (Chloroform)	13			[19]
B21	926 (Chloroform)	1			[19]
B22	823 (toluene)	4			[20]
B23	800 (toluene)	27			[20]
B24	775 (Chloroform)	49			[21]
B25	781 (Chloroform)	50			[21]
B26	791 (Chloroform)	45			[21]
B27	750 (DCM)	45			[22]
B28	805 (Chloroform)	32			[23]
B29	786 (Chloroform)	41			[24]
B30	778 (DCM)	42			[25]
B31	860 (DCM)	24			[25]
B32	782 (Chloroform)	35			[26]

B33	773 (Chloroform)	24	[26]
B34	847 (Chloroform)	14	[26]
B35	853 (Chloroform)	5	[27]
B36	831 (Chloroform)	6	[27]
B37	832 (toluene)	7	[28]
B38	907 (toluene)	13	[28]
Radical	**λ_{PL}[a] (nm)**	**Φ_{sol}[a] (%)**	**Ref.**
R1	800 (toluene)	24	[29]
R2	810 (toluene)	24	[30]
R3	778 (toluene)	66	[31]
R4	783 (cyclohexane)	36	[32]
PB-TPA	770 (toluene)	23	
	833 (Chloroform)	9	
PB-SFA	750 (toluene)	27	This work
	814 (Chloroform)	20	
PB-NSFA	743 (toluene)	31	
	813 (Chloroform)	21	

[a]Measured in solution (λ_{PL} denotes the emission peak and Φ denotes photoluminescent emission efficiency, PLQE);

[b]Measured in a doped film.

The molecules listed from M1 to M19 have been reported within the past 8 years (2017 to 2025) due to the scarcity of neutral, metal-free organic molecules with photoluminescence emission peaks above 770 nm. To date, only a few of these molecules have achieved a PLQE exceeding 20%.

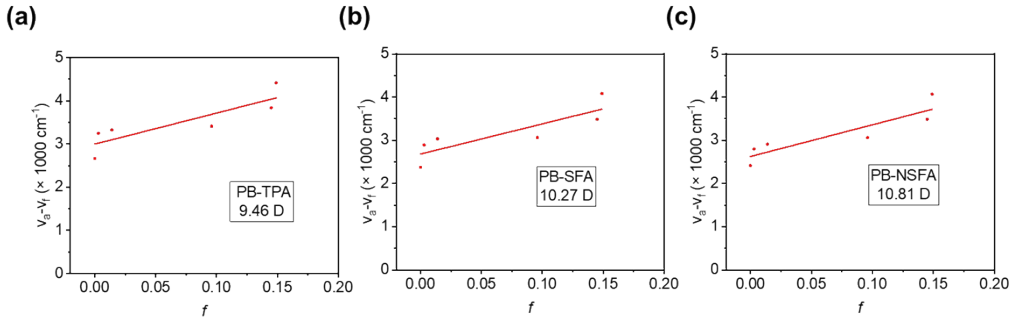

Fig. S21. Lippert-Mataga plot of the Stokes shift (ν_a-ν_f). versus f for (a) PB-TPA, (b) PB-SFA, and (c) PB-NSFA. ν_a and ν_f denote the absorption and fluorescence energies, respectively

Table S3. Photophysical properties of PB-TPA in different solvents.

Solvent	$\triangle f$	ν_a (nm)	ν_f(nm)	ν_a-ν_f (cm^{-1})
Cyclohexane	0	609	727	2665.203
p-Xylene	0.003	612	764	3250.864

Toluene	0.014	613	770	3326.201
Butyl ether	0.096	606	764	3412.645
Isopropyl ether	0.145	605	788	3838.57
Chloroform	0.149	609	833	4415.559

Table S4. Photophysical properties of PB-SFA in different solvents.

Solvent	$\triangle f$	ν_a (nm)	ν_f(nm)	ν_a-ν_f (cm^{-1})
Cyclohexane	0	609	712	2375.417
p-Xylene	0.003	611	742	2889.523
Toluene	0.014	611	750	3033.279
Butyl ether	0.096	608	747	3060.488
Isopropyl ether	0.145	607	770	3487.452
Chloroform	0.149	611	814	4081.6

Table S5. Photophysical properties of PB-NSFA in different solvents.

Solvent	$\triangle f$	ν_a (nm)	ν_f(nm)	ν_a-ν_f (cm^{-1})
Cyclohexane	0	609	714	2414.759
p-Xylene	0.003	611	737	2798.091
Toluene	0.014	611	743	2907.662
Butyl ether	0.096	608	747	3060.488
Isopropyl ether	0.145	607	770	3487.452
Chloroform	0.149	611	813	4066.489

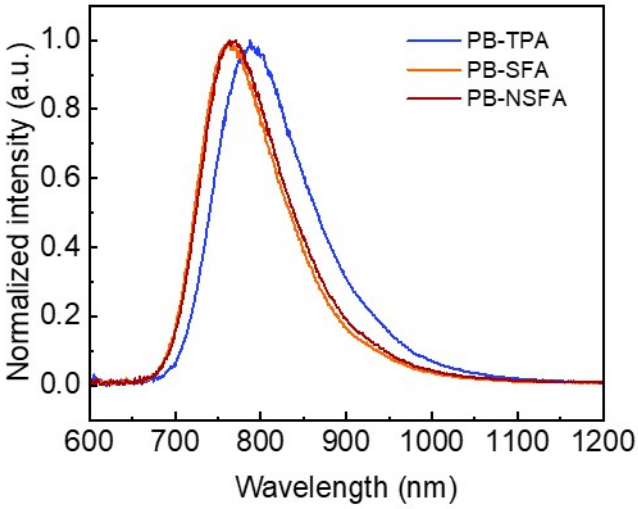

Fig. S22. PL spectra of PB-TPA, PB-SFA, and PB-NSFA in doped MADN films

Table S6. Photophysical properties of three radicals in doped MADN films

	λ_{PL} (nm)	PLQE (%)
PB-TPA	788	4
PB-SFA	764	5
PB-NSFA	771	8

4. Quantum simulations

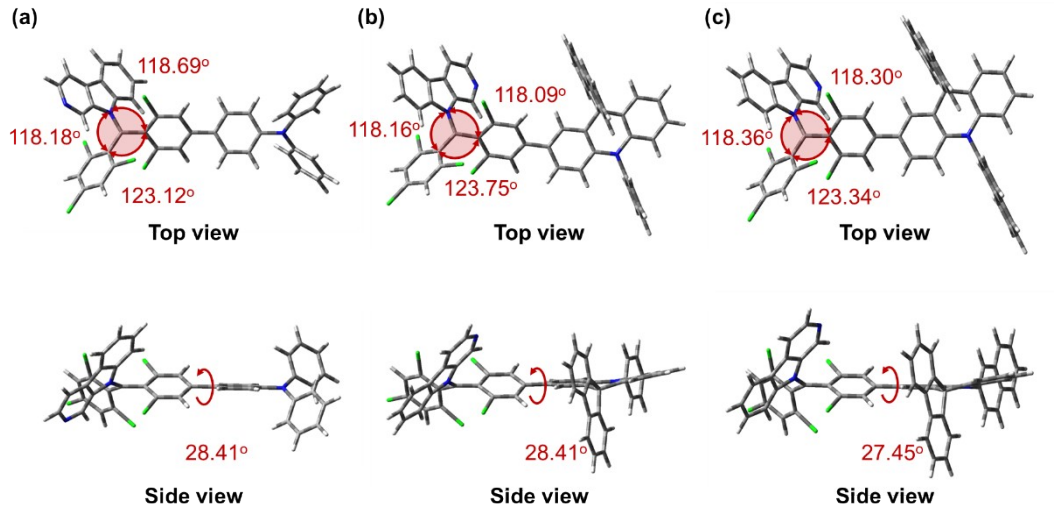

Fig. S23. Optimized ground state configurations of (a) PB-TPA, (b) PB-SFA, and (c) PB-NSFA.

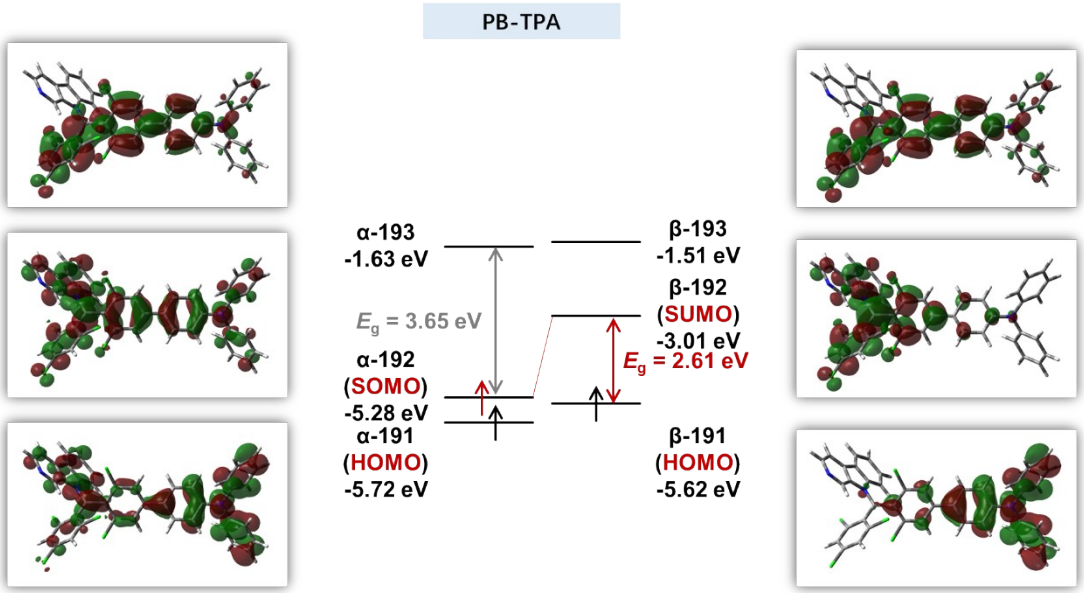

Fig. S24. Orbital distributions and energy levels at the ground state of PB-TPA

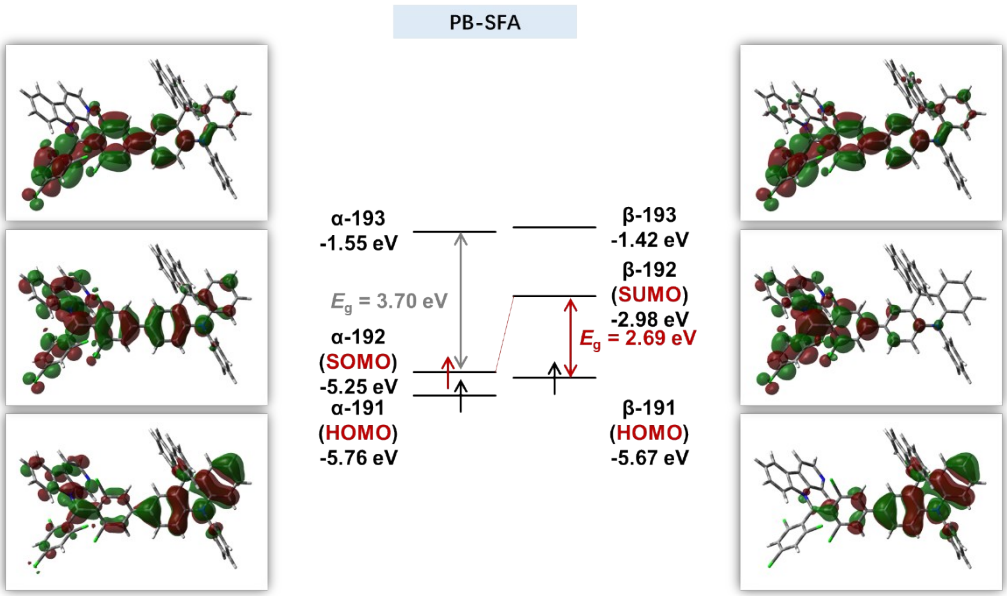

Fig. S25. Orbital distributions and energy levels at the ground state of PB-SFA

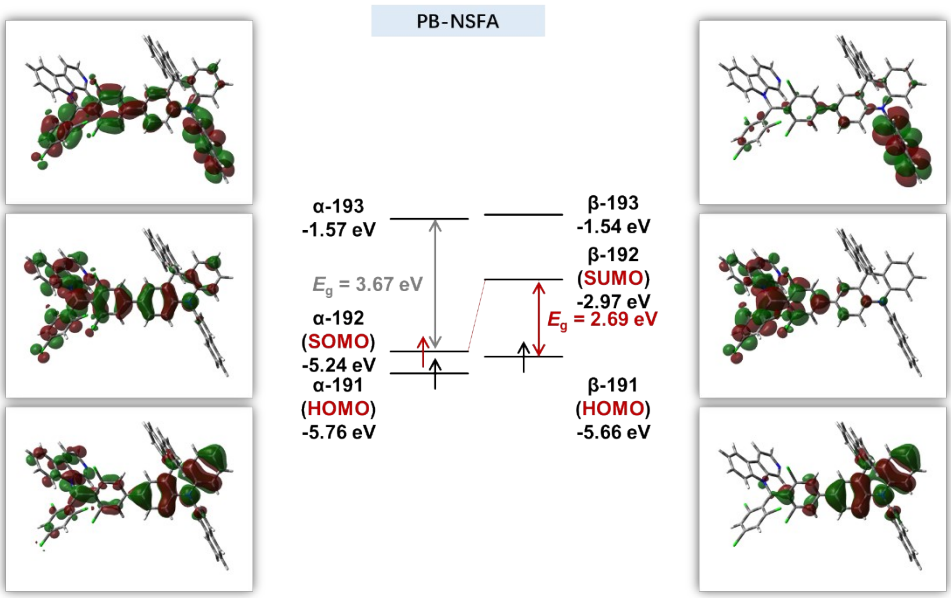

Fig. S26. Orbital distributions and energy levels at the ground state of PB-NSFA

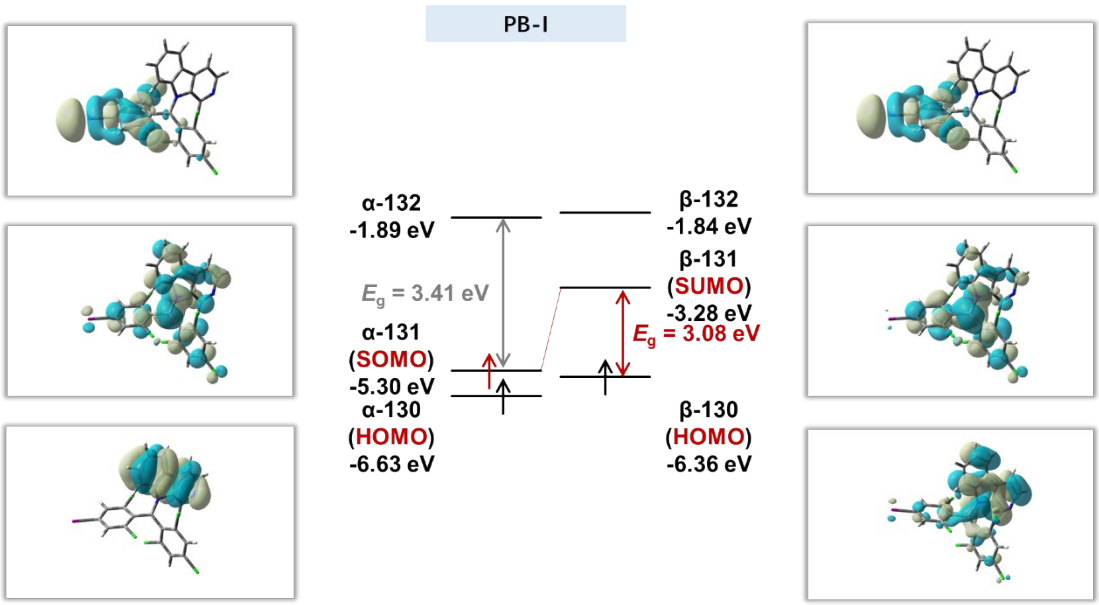

Fig. S27. Orbital distributions and energy levels at the ground state of PB-I

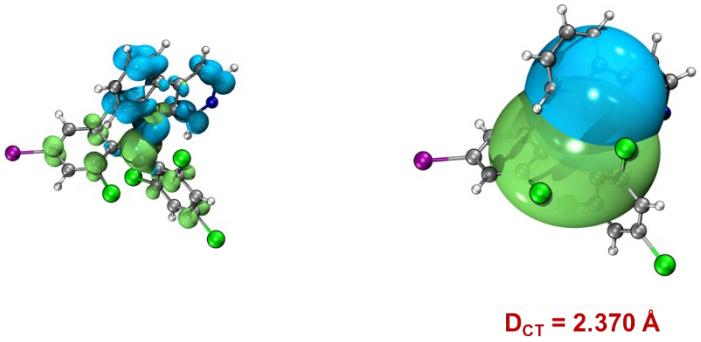

Fig. S28. Hole-electron distributions and charge separation distances of PB-I

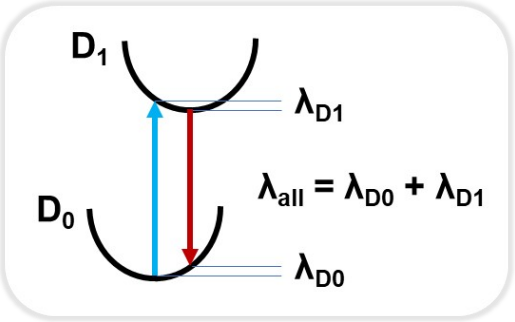

	RMSD	λ_{D0} (eV)	λ_{D1} (eV)	λ_{all} (eV)
PB-TPA	0.2620	0.15	0.22	0.37
PB-SFA	0.1805	0.13	0.20	0.33
PB-NSFA	0.2282	0.14	0.20	0.34

Fig. S29. RMSD and reorganization energy (λ_{all}) of PB-TPA, PB-SFA and PB-NSFA.

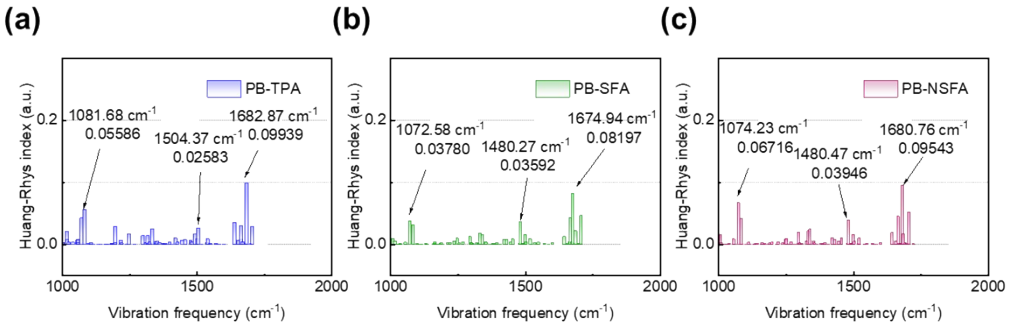

Fig. S30. Huang-Rhys factors for (a) PB-TPA, (b) PB-SFA, and (c) PB-NSFA corresponding to the $D_1 \rightarrow D_0$ transition. (With a zoomed-in view to highlight the region of 1000-2000 cm^{-1}).

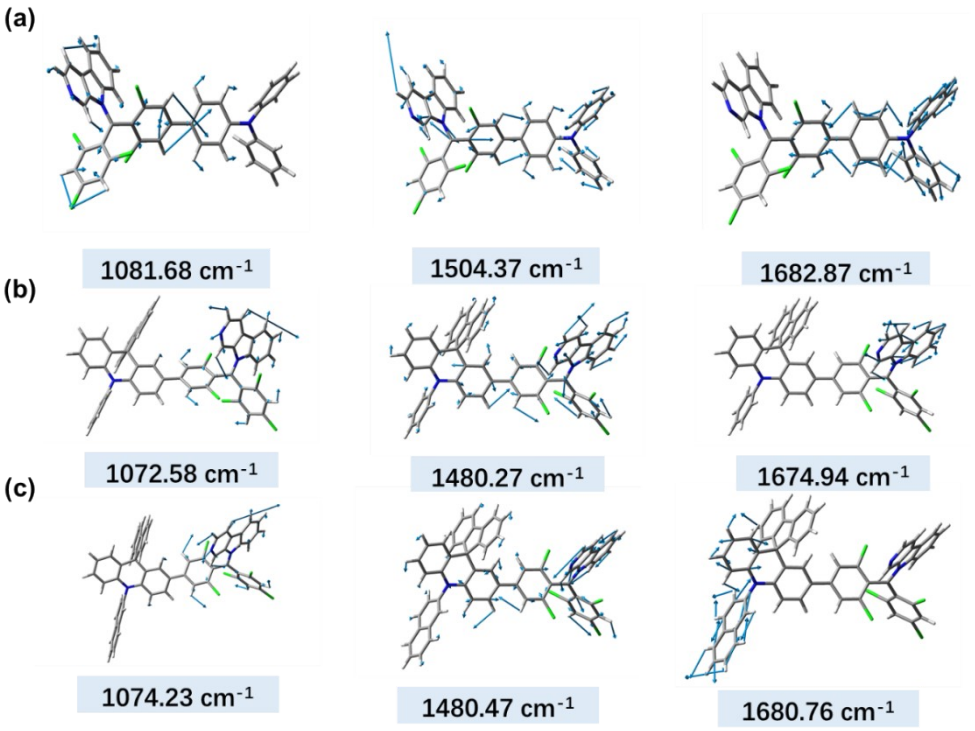

Fig. S31. Vibrations of (a) PB-TPA, (b) PB-SFA, and (c) PB-NSFA in the high-frequency region (The displacement vector is magnified ten times).

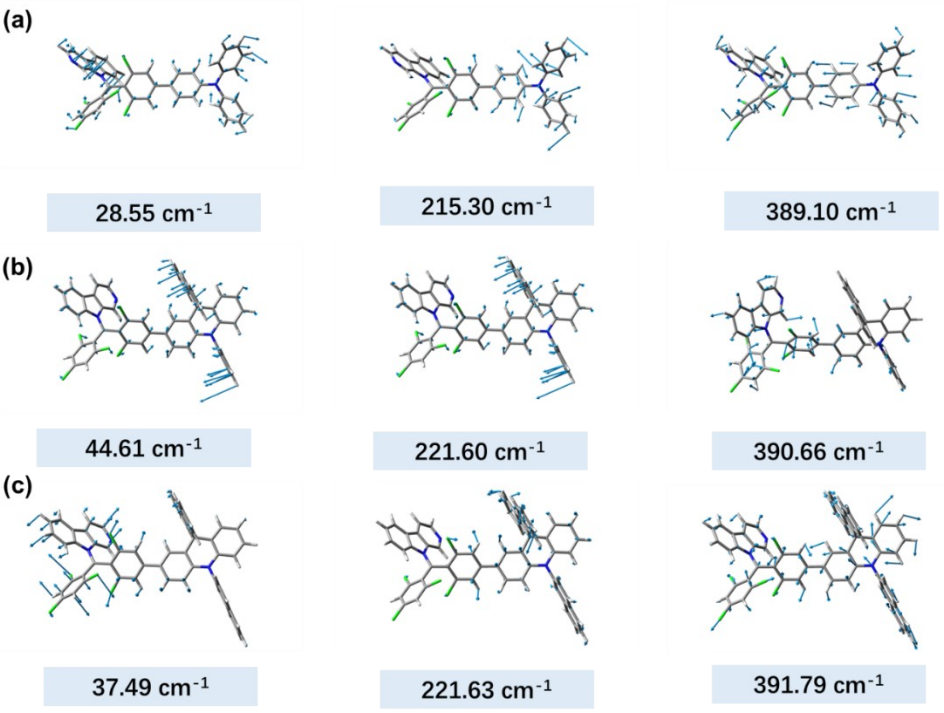

Fig. S32. Vibrations of (a) PB-TPA, (b) PB-SFA, and (c) PB-NSFA in the low-frequency region (The displacement vector is magnified ten times).

5. Reference

[1] M. J. Frisch, G. W. Trucks, H. B. Schlegel, G. E. Scuseria, M. A. Robb, J. R. Cheeseman, G. Scalmani, V. Barone, G. A. Petersson, H. Nakatsuji, X. Li, M. Caricato, A. V. Marenich, J. Bloino, B. G. Janesko, R. Gomperts, B. Mennucci, H. P. Hratchian, J. V. Ortiz, A. F. Izmaylov, J. L. Sonnenberg, Williams, F. Ding, F. Lipparini, F. Egidi, J. Goings, B. Peng, A. Petrone, T. Henderson, D. Ranasinghe, V. G. Zakrzewski, J. Gao, N. Rega, G. Zheng, W. Liang, M. Hada, M. Ehara, K. Toyota, R. Fukuda, J. Hasegawa, M. Ishida, T. Nakajima, Y. Honda, O. Kitao, H. Nakai, T. Vreven, K. Throssell, J. A. Montgomery Jr., J. E. Peralta, F. Ogliaro, M. J. Bearpark, J. J. Heyd, E. N. Brothers, K. N. Kudin, V. N. Staroverov, T. A. Keith, R. Kobayashi, J. Normand, K. Raghavachari, A. P. Rendell, J. C. Burant, S. S. Iyengar, J. Tomasi, M. Cossi, J. M. Millam, M. Klene, C. Adamo, R. Cammi, J. W. Ochterski, R. L. Martin, K. Morokuma, O. Farkas, J. B. Foresman and D. J. Fox in *Gaussian 16 Rev. C.01*, *Vol.* Wallingford, CT, **2016**.

[2] a) T. Lu, *J Chem Phys* **2024**, *161*; b) T. Lu and F. Chen, *J Comput Chem* **2012**, *33*, 580–592.

[3] W. Humphrey, A. Dalke and K. Schulten, *Journal of Molecular Graphics* **1996**.

[4] M. E. Arnold and A. J. C. Kuehne, *Dyes Pigments.* **2023**, *208*.

[5] Q. Yu, Y. Tamura, H. Nakanotani, M. Mamada and C. Adachi, *Adv. Opt. Mater.* **2024**, *12*, 2400932.

[6] X. Zhou, Y. Fan, S. Li, K. Zhang, Y. Pei, Y. Zeng, X. Kang, L. Zhao, H. Chen, Y. Qin, W. Feng, L. Liu and L. Wu, *Nano Lett* **2024**, *24*, 1792–1800.

[7] A. Minotto, P. Murto, Z. Genene, A. Zampetti, G. Carnicella, W. Mammo, M. R. Andersson, E. Wang and F. Cacialli, *Adv. Mater.* **2018**, *30*, 1706584.

[8] Y. Yu, H. Xing, D. Liu, M. Zhao, H. H.-Y. Sung, I. D. Williams, J. W. Y. Lam, G. Xie, Z. Zhao and B. Z. Tang, *Angew. Chem. Int. Ed.* **2022**, *61*, e202204279.

[9] G. Niu, W. Liu, H. Xiao, H. Zhang, J. Chen, Q. Dai, J. Ge, J. Wu and P. Wang, *Chem. Asian J.* **2016**, *11*, 498–504.

[10] H. Lu, S. Shimizu, J. Mack, Z. Shen and N. Kobayashi, *Chem. Asian J.* **2011**, *6*, 1026–1037.

[11] W. Sheng, Y.-Q. Zheng, Q. Wu, Y. Wu, C. Yu, L. Jiao, E. Hao, J.-Y. Wang and J. Pei, *Org. Lett.* **2017**, *19*, 2893–2896.

[12] J. Cui, W. Sheng, Q. Wu, C. Yu, E. Hao, P. Bobadova-Parvanova, M. Storer, A. M. Asiri, H. M. Marwani and L. Jiao, *Chem. Asian J.* **2017**, *12*, 2486–2493.

[13] W. Sheng, J. Cui, Z. Ruan, L. Yan, Q. Wu, C. Yu, Y. Wei, E. Hao and L. Jiao, *J. Org. Chem.* **2017**, *82*, 10341–10349.

[14] S. G. Awuah, J. Polreis, V. Biradar and Y. You, *Org. Lett.* **2011**, *13*, 3884–3887.

[15] Y. Kubota, K. Kimura, J. Jin, K. Manseki, K. Funabiki and M. Matsui, *New J. Chem.* **2019**, *43*, 1156–1165.

[16] Y. Wu, C. Cheng, L. Jiao, C. Yu, S. Wang, Y. Wei, X. Mu and E. Hao, *Org. Lett.* **2014**, *16*, 748–751.

[17] J. Wang, J. Li, N. Chen, Y. Wu, E. Hao, Y. Wei, X. Mu and L. Jiao, *New J. Chem.*

2016, *40*, 5966–5975.
[18] M. Nakamura, H. Tahara, K. Takahashi, T. Nagata, H. Uoyama, D. Kuzuhara, S. Mori, T. Okujima, H. Yamada and H. Uno, *Org. Biomol. Chem.* **2012**, *10*, 6840–6849.
[19] M. Nakamura, M. Kitatsuka, K. Takahashi, T. Nagata, S. Mori, D. Kuzuhara, T. Okujima, H. Yamada, T. Nakae and H. Uno, *Org. Biomol. Chem.* **2014**, *12*, 1309–1317.
[20] J. Wang, Q. Wu, S. Wang, C. Yu, J. Li, E. Hao, Y. Wei, X. Mu and L. Jiao, *Org. Lett.* **2015**, *17*, 5360–5363.
[21] G. M. Fischer, M. K. Klein, E. Daltrozzo and A. Zumbusch, *European Journal of Organic Chemistry* **2011**, *2011*, 3421–3429.
[22] S. Wiktorowski, G. M. Fischer, M. J. Winterhalder, E. Daltrozzo and A. Zumbusch, *Phys. Chem. Chem. Phys.* **2012**, *14*, 2921–2928.
[23] G. M. Fischer, M. Isomäki-Krondahl, I. Göttker-Schnetmann, E. Daltrozzo and A. Zumbusch, *Chem. Eur. J.* **2009**, *15*, 4857–4864.
[24] G. M. Fischer, C. Jüngst, M. Isomäki-Krondahl, D. Gauss, H. M. Möller, E. Daltrozzo and A. Zumbusch, *Chem. Commun.* **2010**, *46*, 5289–5291.
[25] R. Ishimatsu, H. Shintaku, Y. Kage, M. Kamioka, S. Shimizu, K. Nakano, H. Furuta and T. Imato, *J. Am. Chem. Soc.* **2019**, *141*, 11791–11795.
[26] S. Shimizu, T. Iino, A. Saeki, S. Seki and N. Kobayashi, *Chem. Eur. J.* **2015**, *21*, 2893–2904.
[27] Y. Kage, H. Karasaki, S. Mori, H. Furuta and S. Shimizu, *ChemPlusChem* **2019**, *84*, 1648–1652.
[28] W. Sheng, Y. Wu, C. Yu, P. Bobadova-Parvanova, E. Hao and L. Jiao, *Org. Lett.* **2018**, *20*, 2620–2623.
[29] H.-H. Cho, S. Kimura, N. C. Greenham, Y. Tani, R. Matsuoka, H. Nishihara, R. H. Friend, T. Kusamoto and E. W. Evans, *Adv. Opt. Mater.* **2022**, *10*, 2200628.
[30] K. Lv, M. Zhang and F. Li, *J. Mater. Chem. C.* **2023**, *11*, 15892–15897.
[31] C. Wu, C. Lu, S. Yu, M. Zhang, H. Zhang, M. Zhang and F. Li, *Angew Chem Int Ed Engl.* **2024**, *63*, e202412483.
[32] M. Zhang, Y.-J. Yu, Z. Dai, W. Wang, H. Zhang, M. Zhang and F. Li, *J. Am. Chem. Soc.* **2025**, *147*, 45423–45431.